Failure modes of electrospun nanofibers

E. Zussman,[a] D. Rittel, and A. L. Yarin
Faculty of Mechanical Engineering, Technion-Israel Institute of Technology, Haifa, 32000, Israel

(Received 21 January 2003; accepted 25 March 2003)

Failure modes of electrospun polymer nanofibers are reported. The nanofibers have diameters in the range of 80–400 nm and lengths greater then several centimeters. The nanofibers fail by a multiple necking mechanism, sometimes followed by the development of a fibriliar structure. This phenomenon is attributed to a strong stretching of solidified nanofibers by the tapered accumulating wheel (electrostatic lens), if its rotation speed becomes too high. Necking has not been observed in the nanofibers collected on a grounded plate. © *2003 American Institute of Physics.*
[DOI: 10.1063/1.1579125]

The present work deals with failure modes of solidified polymeric nanofibers, with diameters in the range of 80–400 nm obtained via electrospinning. Observations clearly show multiple necking formation and fragmentation at a high rate of stretching of the nanofibers. The results clearly distinguish nanofibers from macroscopic metal or polymer specimens where multiple necking is seldom reported as a failure mode. The reason is that typically macroscopic specimens cannot accommodate more than a single neck, while nanofibers can.

In the electrospinning process, a jet of polymer solution is ejected from the tip of a droplet under the action of electrostatic forces.[1–6] The as-spun nanofibers typically form a nonwoven mat. Individual nanofiber sections of lengths of the order of several centimeters can be sorted out and collected.[7]

The electrospinning process is characterized by elongation rates of the order of $\dot{\gamma}=1000\ \mathrm{s}^{-1}$ and cross-sectional area reduction as large as 10^6,[3] which correspond to the logarithmic strain of material elements of the order of 10. The typical polymer solutions have relaxation times of the order of $\theta\sim 0.01-0.1$ s. Therefore, the product $\dot{\gamma}\theta \sim 10^1-10^2$ is much larger than the de Gennes[8] threshold of the strong stretching of 1/2. Under such conditions, stretching and axial ordering of the macromolecular coils should happen, resulting in flow-induced crystallization.[9]

Electrospinning of oriented nanofibers from poly(esters) and poly(aramids) were investigated in Ref. 1, while Ref. 10 addresses oriented nanofibers of 1% poly(ethylene) solution. These nanofibers displayed a fibrillar crystal structure reminiscent of the familiar shish-kebab morphology. Atomic force microscopy (AFM) was used to investigate electrospun poly(ethylene oxide) nanofibers.[11] Some evidence of molecular orientation parallel to the fiber axis was found. A fibrillar structure of nanofibers electrospun from a silk-like polymer with Fibronectin functionality was reported in Ref. 12. The fibrillar structure was oriented along the fiber axis and consistent with the AFM studies of Ref. 11. The fibrillar structure consisted of whisker-like-structures of the order of 12 nm wide. Oriented nanofibers should also be birefringent, as shown experimentally in Ref. 13.

In the present work, poly(ethylene oxide) (PEO) $\{[-(CH_2)_2-O-]_n\}$, with an average molar mass of $M_W=6\times10^5$ g/mol (Aldrich), was used to prepare 2 and 7 wt % aqueous solutions (with 40% ethanol). PEO with $M_W=10^6$ g/mol (Aldrich) was used to prepare a 4 wt % aqueous solution (with 40% ethanol). The polymer solutions were held in a plastic syringe with tip inner diameter of 0.6 mm. A pendant droplet of polymer solution was sustained at the syringe tip.

The jet issued downwards from the tip of the pendant drop of polymer solution and was attracted towards the sharp edge of a collector disk rotating around a horizontal axis. The edge was placed at a distance of 200 mm below the droplet (cf. Ref. 7 for more detail). The disk, of diameter $D=200$ mm, was made of aluminum and had a tapered edge with a half-angle of 26.6°, to create a strong converging electrostatic field (electrostatic lens). As a result, an electric potential difference of approximately 10 kV was created between the surface of the liquid drop and the rotating disk collector. All the experiments were performed at ambient temperature (25 °C) in room air. As the electric potential difference between the droplet and the grounded wheel increased, the droplet acquired a cone-like shape. At a certain potential difference, an intact jet issued from the cone and moved downward toward the wheel. Initially, the jet flowed away from the droplet in a nearly straight line, after which it bent into a complex path that can be bounded by a conical envelope. Then, at a certain point above the wheel, the envelope cone started to shrink, resulting in an inverted envelope cone with its apex touching the wheel's edge. During the spinning process, the disk was rotated at a constant speed as it collected the developing nanofibers on its sharp edge. The linear speed on the edge of the disk collector was $V=5.3$ m/s. As the nanofiber reached the wheel, it was wound around the edge. A significant part of the nanofiber length was captured by the wheel. This is supported by experimental observations and the following estimate. For a jet velocity of the order of $V_t=10^{-1}$ cm/s at the droplet tip a length of $\ell_t=10^{-1}$ cm enters the jet during 1 s. The nanofiber length of $\ell_w=\ell_t(a_t/a_w)^2c_p$ arrives at the wheel during 1 s due to polymer mass conservation (a_t and a_w are the fiber cross-sectional radii at the droplet tip and the wheel, respectively, and c_p is the initial polymer concentration). For $a_t=10^{-2}$ cm, $a_w=10^{-5}$ cm and $c_p=0.02$, $\ell_w=20$ m. On the

[a]Electronic mail: meeyal@tx.technion.ac.il

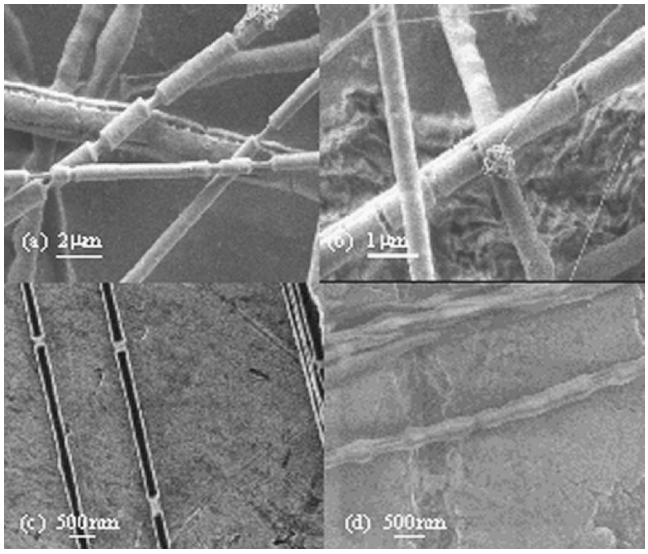

FIG. 1. Electron micrographs of multiple neck formation in electrospun nanofibers. (a) and (b) 7% PEO electrospun nanofibers, (c) and (d) 4% PEO electrospun nanofibers.

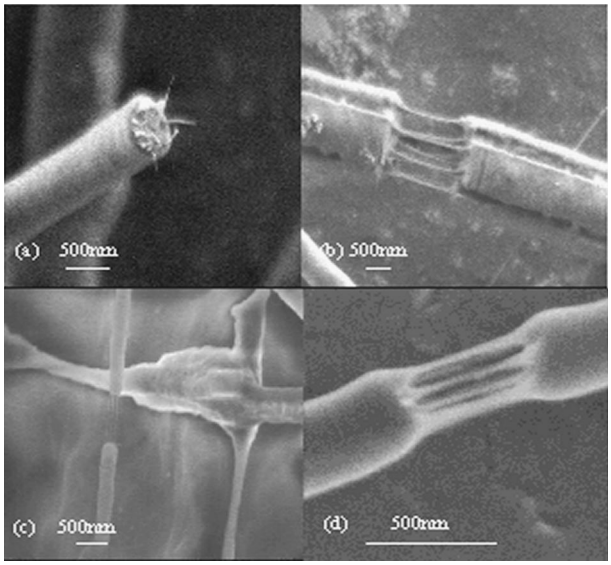

FIG. 2. Electron micrographs of fibrillar structures. (a) failed 7% PEO electrospun nanofiber, (b) fibrillar structure in 7% PEO electrospun nanofiber, (c) and (d) fibrillar structures in 4% PEO electrospun nanofibers.

other hand, the wheel can accommodate 5.3 m of nanofiber during 1 s. The fact that this value is less than that of ℓ_w means that nanofiber can be folded at the wheel.

An aluminum stub (5×4 mm^2) covered with conductive carbon tape, or a microscope glass slide, was attached to the disk edge to facilitate both the collection of the nanofibers and their subsequent removal. The morphology of the electrospun nanofibers was observed with a high-resolution scanning electron microscope (HR–SEM) (Leo Gemini 982). The diameter of the nanofibers was measured using the atomic force microscope (AFM), Nanoscope III (Digital Instruments) in tapping mode. AFM scans were performed in air, utilizing Si_3N_4 cantilever (Nanotips, Digital Instruments).

Wide angle x-ray diffraction (WAXD) photographs were taken, using Ni-filtered Cu K_α radiation. A pinhole collimator was used. Both the fiber axes and the flat photographic films were perpendicular to the x-ray beam. The electrospun nanofibers used as a sample in the WAXD experiments were collected by means of the earlier-mentioned electrostatic lens, at the edge of the wheel in the form of a microrope. The rope was removed from the wheel and wrapped around a 0.3 mm thick metal frame. The polymer sample thickness was about 1 mm in order to minimize the exposure time.

As a control experiment, nanofibers were also electrospun with similar electrostatic field strength onto an aluminum plate that served as a grounded collector. The nanofibers collected on the aluminum plate, from all the earlier-mentioned polymers, formed a nonwoven mat.

SEM examinations of nanofibers collected on the rotating wheel revealed multiple necking patterns at certain places along the nanofibers, as shown in Fig. 1. In Fig. 1(a), nanofibers electrospun from 7% PEO solution are shown. The fiber diameter contracted from 320 nm to nearly 60 nm in the neck regions. The necks were not evenly spaced along the nanofibers, and the distance between them varied between 1 and 7 μm. Figure 1(b), also shows nanofibers electrospun from 7% PEO solution, with thin fibrillar structures visible in the neck regions. The fibrils are only weakly bonded together and in some places are separated. Figures 1(c) and 1(d), show nanofibers electrospun from 4% PEO solution, with distance between the necks of 4–6 μm. Also in these cases fibrillar structures are visible in the neck regions. This is similar to crazing often observed in cracking of polymers.

In Fig. 2, several examples of fibrillar structures of the nanofibers are shown in more detail. In Fig. 2(a), a failed single nanofiber electrospun from 7% PEO solution, is shown. Several fibrils are sticking out from the nanofiber cross section. The estimated diameter of the nanofiber is of about 550 nm, whereas a single fibril diameter is about 20 nm. Figure 2(a) also seemingly shows that the nanofiber has a compact shell and a rarefied core with fibrils. Such a structure could appear as a result of a fast solvent evaporation. In Fig. 2(b), a nanofiber electrospun from 7% PEO solution is shown. The nanofiber diameter is in the range of 800–1000 nm, whereas its fibril diameters are of about 80 nm. Figures 2(c) and 2(d) depict electrospun nanofibers made of 4% PEO solution with clearly separated fibrils. In this case, the nanofiber diameter is about 250 nm, which is, as expected, smaller than that of the 7% PEO solution nanofibers. The fibril diameters here are of about 20 nm. Note that this width is reminiscent of the fibrillar structure observed in Refs. 11–13. It is also very close to the thickness of the extended chain crystals of poly(ethylene oxide), which can be folded, revealed in Ref. 14. Small-angle x-ray scattering could not reveal any additional information. Some of the nanofibers appear to have large beads, formed by capillary instability or due to poor control of the polymer flow rate during the electrospinning process.

An AFM image of a single 2% PEO electrospun nanofiber on a glass slide is shown in Fig. 3. Measurements of the nanofiber diameter in the necking region revealed an abrupt contraction of the cross-sectional diameter from 225 to 26 nm. The AFM image unambiguously shows genuine necking of the nanofiber. This observation excludes the possibility of nanofiber disruption or thinning by the electron beams dur-

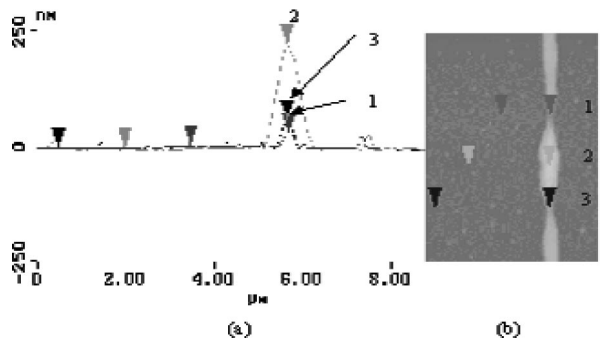

FIG. 3. AFM image of electrospun nanofiber made of 2% PEO solution. (a) Maximum height at cross section 1 is 52 nm, at cross section 2 is 225 nm, and at cross section 3 is 26 nm. (b) Top view of the measured nanofiber.

ing SEM analysis. Figure 4 is a WAXD pattern obtained for a PEO nanofiber microrope. The pattern shows six diffraction arcs with a high degree of orientation (texture). Analysis of this pattern leads to a monoclinic crystalline structure of PEO with helical molecular conformation.[15]

The results obtained in the present work reveal that the PEO nanofibers fail by multiple necking and in certain cases crazing of the necked regions is visible. These observations have been obtained only for nanofibers that were wound around the sharp edge of a rotating wheel. On the other hand, nanofibers that were collected on the aluminum plate were not subject to tension (while the ones collected on the wheel were stretched) and did not demonstrate any failure mode. Their diameters vary in the range of 80–700 nm and lengths of up to several centimeters.

As we have shown, necking is characteristic of only the nanofibers accumulated at the sharp edge of a rotating wheel, and not of those collected on the grounded plate. Therefore, stretching of the almost solidified nanofibers by the rotating wheel could be seen as the source of necking. Later we show that in distinction from macroscopic polymer specimens nanofibers can accommodate more than a single neck. The rate of stretching of solidified polymer nanofiber attached to the wheel is of order of $2V/D=53\ \mathrm{s}^{-1}$, i.e., rather high.

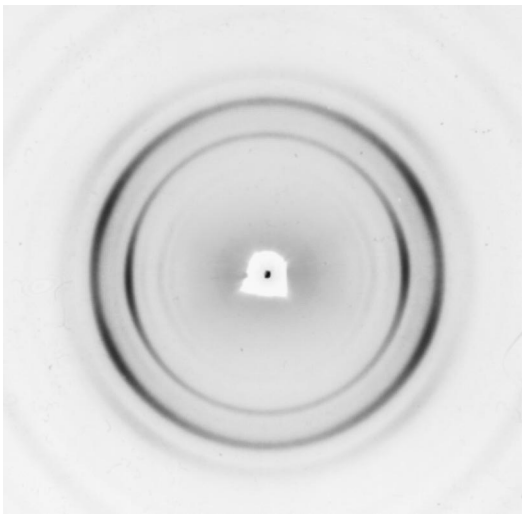

FIG. 4. Typical x-ray pattern of the oriented nanofiber rope made of 6% PEO ($M_W=600\,000$ g/mol) aqueous solution with 40% ethanol.

Under such conditions single necking of macroscopic cylindrical polymer samples, is most likely to be the dominant failure mode. Due to the fact that nanofibers possess aspect ratios (length to diameter ratio) much higher than those of macroscopic polymer samples, they can accommodate many perturbation wavelengths, which leads to multiple necking. According to the observations, the wavelength of the instability leading to multiple necking on the nanofibers is of the order of $\ell_0=5\ \mu$m. For a nanofiber of cross-sectional diameter of the order of $d_0=100$ nm, the wavelength to diameter ratio is of the order of $\ell_0/d_0=50$. One can speculate that the same ratio should correspond to necking of macroscopic polymer specimens, where d_0 is typically of the order of 0.5 cm. Then the internecking spacing expected becomes about 25 cm, which is of the order of the full length of such specimens. That is the reason that macroscopic polymer specimens cannot accommodate more than a single neck, as we have checked experimentally in the present work in addition to the experiments with nanofibers.

To summarize, the two main modes develop sequentially. The first mode is multiple necking, that is sometimes followed by development of a fibrillar structure in the necked regions. The failure modes found indicate a large ductility of the solidified, partly crystalline fibers. The results obtained show that the source of necking is strong stretching of solidified nanofibers by the tapered wheel, if its rotation speed becomes high enough. This conclusion is supported by the fact that necking was not observed in nonwoven nanofiber mats collected on a grounded plate. The uneven diameter and charge distribution along the electrospun jet is assumed to be the trigger of the growing perturbations leading to the formation of multiple necks on electrospun nanofibers.

The authors acknowledge the support of this research by the Israel Science Foundation, the Israel Academy of Sciences, Grant No. 287/00-1. This research was also supported by the Fund for the Promotion of Research at the Technion. Dr. M. H. Berger is kindly acknowledged for her assistance with SEM work. Dr. R. Khalfin is kindly acknowledged for his assistance with x-ray work.

[1] D. H. Reneker and I. Chun, Nanotechnology **7**, 216 (1996).
[2] H. Fong and D. H. Reneker, in *Structure Formation in Polymer Fibers*, edited by D. R. Salem and M. V. Sussman (Hauser, Munich 2000), p. 225.
[3] D. H. Reneker, A. L. Yarin, H. Fong, and S. Koombhongse, J. Appl. Phys. **87**, 4531 (2000).
[4] A. L Yarin, S. Koombhongse, and D. H. Reneker, J. Appl. Phys. **89**, 3018 (2001).
[5] M. Bognitzki, W. Czado, T. Frese, A. Schaper, M. Hellwig, M. Steinhart, A. Greiner, and J. H. Wendorff, Adv. Mater. (Weinheim, Ger.) **13**, 70 (2001).
[6] J. M. Deitzel, J. D. Kleinmeyer, J. K. Hirvonen, and N. C. B. Tan, Polymer **42**, 8163 (2001).
[7] A. Theron, E. Zussman, and A. L. Yarin, Nanotechnology **12**, 384 (2001).
[8] P. G. De Gennes, J. Chem. Phys. **60**, 5030 (1974).
[9] A. Ziabicki, Colloid Polym. Sci. **277**, 752 (1999).
[10] L. Larrondo and R. J. Manley, J. Polym. Sci., Polym. Phys. Ed. **19**, 909 (1981).
[11] R. Jaeger, H. Schonherr, and G. J. Vancso, Macromolecules **29**, 7634 (1996).
[12] C. J. Buchko, L. C Chen, Y. Shen, and D. C. Martin, Polymer **40**, 7397 (1999).
[13] H. Fong and D. H. Reneker, J. Polym. Sci., Part B: Polym. Phys. **37**, 3488 (1999).
[14] S. Z. D. Cheng, H. S. Bu, and B. Wunderlich, Polymer **29**, 579 (1988).
[15] Y. Takahashi and H. Tadokoro, Macromolecules **6**, 672 (1973).